Comparison of rolling contact fatigue life between elastohydrodynamic lubricated point contacts pre and post running-in treatment

Hui Cao[1], Zulfiqar Khan[2] and Yonggang Meng[1*]

[1]State Key Laboratory of Tribology, Tsinghua University, Beijing 100084, China

[2]NanoCorr, Energy and Modeling (NCEM) Research Group, Department of Design & Engineering, Bournemouth University, Talbot Campus, Fern Barrow, Poole, BH12 5BB, United Kingdom

[*]Corresponding author: mengyg@tsinghua.edu.cn

Abstract: *Rolling contact micropitting fatigue life is affected by stress fields in shallow subsurface. It is well known that there is a significant dependence, of stress distribution in subsurface, on the surface microstructures. Therefore rolling contact micropitting fatigue lives can be enhanced through modifying surface topography. In this study, running-in method was employed as the method to alter surface microstructures to explore the effect of various morphological characteristics on micropitting fatigue lives. Firstly, various rough surfaces were formed by applying experimental running in processes on a series of ball-on-disc pairs. Meanwhile, the evolutions of topography during the running-in processes were recorded. Secondly, rolling contact fatigue lives of these rough surfaces under elastohydrodynamic lubricated condition were calculated and compared based on Zaretsky's fatigue model combined with elastic contact mechanics. The results have indicated that a running-in process has significantly positive effect on prolonging micropitting fatigue lives. Theoretical analysis of the relationship between topographical parameters and micropitting fatigue lives to ascertain optimum morphological characteristics which are beneficial in reducing micropitting fatigue failures is the key originality of this work. This work provides guidelines on surface morphology for achieving maximum pitting fatigue life for interacting systems. In turn enhanced durability of the systems will lead to significant cost savings.*

Keywords: *Rolling Contact, Micropitting, Fatigue Life, Running-in, Morphological Characteristics, Model, Simulation*

Nomenclature

R_q = root mean square roughness, m

r_s = average radius of asperities, m

W = load, N

U_e = average entrainment speed, m/s

η_0 = original dynamic viscosity of oil, Pa.s

η = dynamic viscosity of oil under high pressure, Pa.s

E_1, E_2 = elastic modulus of ball and disc, GPa

E = equivalent elastic modulus, GPa

G = equivalent shear modulus, GPa

v_1, v_2 = Poisson's ratio of ball and disc

ρ_0 = original density of lubricant, Kg/m^3

ρ = density of lubricant under high pressure, Kg/m^3

x = entrainment speed direction, m

y = direction perpendicular to entrainment speed, m

R_x = equivalent radius of ball in entrainment speed direction, m

R_y = equivalent radius of ball in direction perpendicular to entrainment speed, m

h = film thickness, m

h_0 = original gap between ball and disc, m

v_e = elastic deformation, m

ψ = surface height of disc, m

f = shear stress between ball and disc, m

p_f = fluid pressure, Pa

p_c = pressure between solid or boundary film, Pa

τ_L = character shear stress of lubricant, 18MPa

τ = shear stress of compressed fluid, Pa

S = survival probability of material

A = material coefficient, 1×10^{-10}

c = stress index

e = Weibull slope

τ_{vm} = equivalent von Mises stress, Pa

V = stress volume, m^3

X, Y, Z = position coordinates, m

ζ, ξ = position coordinates, m

σ_{mn} = contact stress component, Pa

m, n = 1,2,3, subscripts represent three stress directions,

i, j, k, q, l = 1,2,3…, subscripts represent discrete counting variables

s = sliding to rolling ratio

a = Hertz contact radius, m

v = Poisson's ratio of material

K = equivalent curvature of asperity, 1/m

I = x, y, subscripts represents two directions

K_I = curvature of asperity in the I direction, 1/m

z = height of asperity, m

t = number of asperity

$r_{s,t}$ = radius of the tth asperity, m

Q = total number of asperities

1. Introduction

Rolling contact fatigue failure is a major concern in many engineering applications. There are many factors that affect rolling contact fatigue lives, such as lubrication conditions, surface roughness, contact loads and contact geometry. All these factors influence the equivalent shear stress distribution in the subsurface, which is the key factor leading to materials' fatigue. Rolling contact fatigue spalling is a major failure mode in engineering applications within industry. This leads to large exfoliations peeled from the surface [1]. This contact fatigue is mainly influenced by the Hertz stress distribution on the contacting surfaces. Therefore, spalling fatigue is determined by the total load, elasticity and curvatures of the rolling contact surfaces. Micropitting fatigue is another common failure mode of rolling contacts, which has a significant influence on the

operation behavior in precision mechanical components such as precision rolling bearings. Therefore it has attracted the attention of industry professionals, scientists and researchers. The mechanism of micropitting fatigue is that cracks are generated in very shallow positions within subsurface and then gradually propagate to surface with the formation of small debris [2]. The depth of a micropitting defect is usually up to 50 micrometers [3]. Hence, micropitting fatigue failure is mainly determined by the shallow stress distributions. Many researchers have indicated that the stress distribution in shallow subsurface has a close relation with surface topography while that in deep subsurface it is usually determined by the maximum Hertz contact stress. Therefore, it has the potential to improve pitting fatigue lives by changing the surface topography. Running-in is a commonly used method to modify surface roughness. It is therefore employed in this study to generate different rough surfaces to explore the optimum topographical characteristics which will enable prolonging micropitting fatigue lives.

Rolling contact fatigue life estimation methods have been developed over the past several decades. The most famous L-P model was proposed by Lundberg and Palmgren in 1940s to predict fatigue lives of rolling bearings [4], which is still applicable in terms of adoptive criterion in bearing design. Theoretical emphasis of this model is on the correlation of stress volume and the maximum number of contact stress cycles before fatigue occurs at a certain survival probability level of the material. It could easily be found from the L-P model that fatigue life is always finite at any stress level given that the stress cycle number is large enough. Later in 1970s, Harris and Ioannides stated that fatigue would not occur for extremely long operated duration in rolling bearings if maximum contact stress is below a critical value. Therefore they revised L-P law by introducing a material fatigue strength limitation in the model [5]. The denominator (H) tends to approach a minimum value to a zero, when extremely high stresses are concentrated close to the surface, in this case I-H model lose its efficacy. In order to improve this limitation, Zaretsky et al. proposed a new model in 1980s to predict fatigue life based on the original Weibull theory. This was further based on a series of various materials and non-rolling contact fatigue experimental data [6-8]. In this model, the fatigue limitation and the stress depth items are abandoned, this method is also efficient for utilization where contact surfaces are rough or there are complicated stress

distributions. Recently, Zhu and Wang et al. applied Zaretsky model in predicting line contact tribo-pairs under mixed lubrication and the results corresponded well with the experiments [9].

According to the above fatigue models, the stress fields in the subsurface need to be obtained when predicting rolling contact fatigue life of lubricated ball on disc pair. Moreover, it is well known from contact mechanics that stress fields within the subsurfaces are determined by the contact pressure on surfaces. Therefore, it is necessary to solve the elastohydrodynamic lubrication problems to obtain the pressure distributions.

Over the past several decades, great efforts have been made to explore solving elastohydrodynamic lubrication problems. Dowson and Hamrock investigated elastohydrodynamic lubrication issues within the context of ideally smooth circular contacts under low load and medium speed conditions [10]. Later, other researchers have developed numerical methods to solve Reynolds equation and expanded smooth surfaces solutions to high load, high speed and ultralow speed [11-13]. It was at the end of 1970s that the most famous statistical average flow model was proposed by Patir and Cheng to simulate hydrodynamic lubrication behavior of sliding rough surfaces [14, 15]. In 2015, M.M. Khonsari combined this model with statistical contact mechanics model and presented systematic mixed-lubrication solutions of line contacts and point contacts [16, 17]. However, statistical mixed lubrication solutions do not have the capacity to describe real micro lubrication behaviors of tribo-pair, as all pressures and film thickness results are averaged within the contact region. Hu and Zhu have developed a unified Reynolds' equation to solve the mixed lubrication problem [18-23], which is called deterministic model. In this model, surface height data is considered in the original gap between the contact pair and the film thickness results can clearly distinguish the solid to solid contact zones from micro hydrodynamic lubricated zones all over the whole contact region. Moreover, the pressure results predicted by this model are also correlated with the surface height variation, which reflects the pressure mapping in the mixed lubricated regime. In the present study, the deterministic mixed lubrication model was employed to predict detailed pressure and film thickness distributions.

Based on the above survey, the main contents in this study are summarized as follow; (i) running-in process for each tribo-pair was scheduled on a bench tribo-testing under

mixed lubrication condition to obtain rough surfaces with various topographies. (ii) surface parameters of running-in regions on these discs were characterized and compared. (iii) rolling contact fatigue lives of discs under rolling contact elastohydrodynamic lubricated condition were numerically estimated and compared by introducing Zaretsky model and elastic contact mechanics. (iv) the effect of running-in to improve rolling contact pitting fatigue lives was theoretically explained by comparing the distributions of the contact pressures and subsurface stress fields. (v) R_q and mean asperity radius r_s of surfaces were statistically analyzed to explore the relations between micropitting fatigue life and these topography parameters. Finally, R_q/r_s was proposed as a key morphology parameter that affects the micropitting fatigue lives of rough surfaces.

2. Formation of surfaces with various topographies based on experimental running-in method

2.1 Specimens and Lubricants

Five sets of AISI 52100 steel balls and discs were prepared as the tribo-pairs in running-in series to generate different topographies. All the balls are of the same specification with diameter of 12.7mm and a root mean square roughness of 0.014μm. Five discs with different initial surface textures and roughness were prepared. Three-dimensional morphologies of the discs are provided in figure 1. For case 1, case 2 and case 5, the texture orientation is 45 degrees in respect to sliding direction while the root mean square roughness values are 0.059μm, 0.56μm and 0.174μm, respectively. For case 3 and case 4, the root mean square roughness values are almost the same as case 5 while the surface texture are longitudinal (0 degree) and transverse (90 degrees) in respect to sliding direction, respectively. A ball on disc configuration has been used in this study. An upper ball is fixed in a collet with zero degrees of freedom during running-in tests. The disc was fixed on the reciprocating platform as a lower sample. PAO6 base oil, free of any additives, with purity of 99% and viscosity of 48 mPa.s (303K) was selected as lubricant.

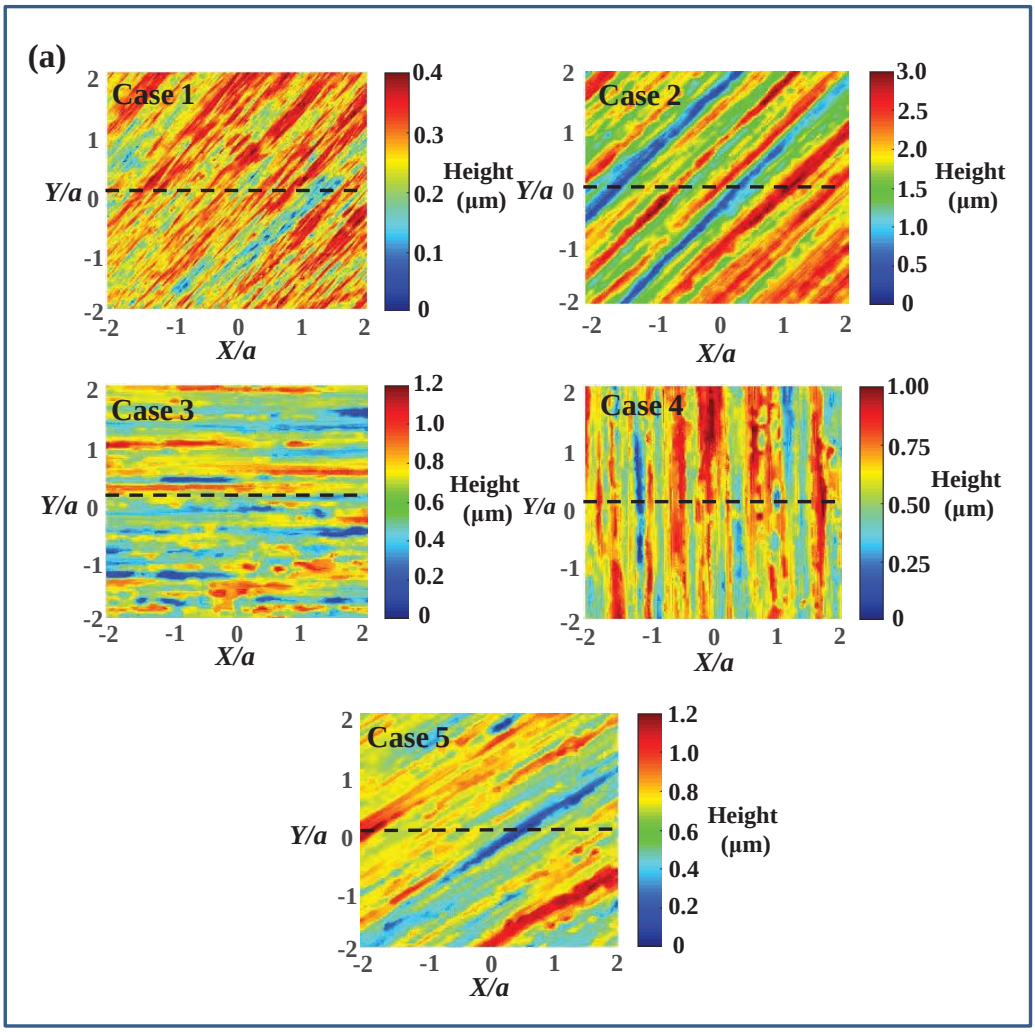
(a)
Case 1
Case 2
Case 3
Case 4
Case 5
Y/a
X/a
Height (μm)
0.4
0.3
0.2
0.1
0
3.0
2.5
2.0
1.5
1.0
0.5
1.2
0.8
0.6
1.00
0.75
0.50
0.25
2
1
0
-1
-2

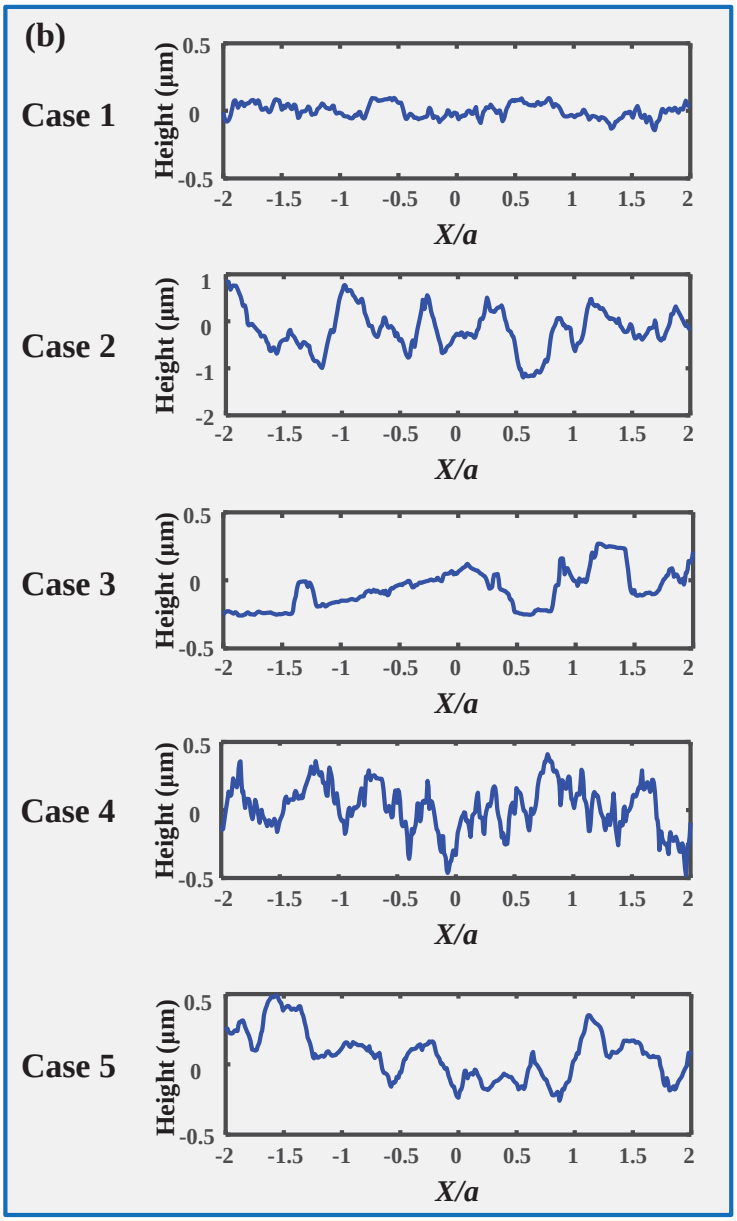

Fig. 1 Original Morphology of Five Rough Surfaces. (a) 3D morphological image. (b) Cross section profile of each case. Here, a=151μm is the Hertz contact radius by applying a load of 80N to 52100 steel ball-on-disc contact pair. Case 1, orientation 45 degrees, R_q 0.059μm; Case 2, orientation 45 degrees, R_q 0.56μm; Case 3, orientation 0 degree, R_q 0.172μm; Case 4, orientation 90 degrees, R_q 0.174μm; Case 5, orientation 45 degrees, R_q 0.174μm.

2.2 Detailed procedures and operating parameters of running-in process

Schematic diagram of tribo-test system is shown in figure 2. In order to study the topography evolutions of the same local region on the disc with and without a running-in duration, start-stop frictional tests were performed for all friction pairs. The running-in procedure is similar to that used in the previous study [24], briefly described as follow; (i) one local region on the disc was selected as a carrier to study the friction and wear behaviors in a running-in course. Before running-in starting, original topography of this region was measured on the profilometer attached on the tribo-bench testing rig. Then the running-in started with oil fed in the contact region. The running-in was terminated after 576 seconds at which the monitored friction coefficient reached a steady value. After the lubricant and wear debris attached to the disc and the ball were cleaned by flushing acetone, the disc held on the platform was moved from the rubbing position to the measurement position for white light profilometer analysis to measure the rubbed region. For all the five cases, the same running-in period as abovementioned was conducted. The operating conditions and mechanical properties of the ball and disc material are listed in Table 1.

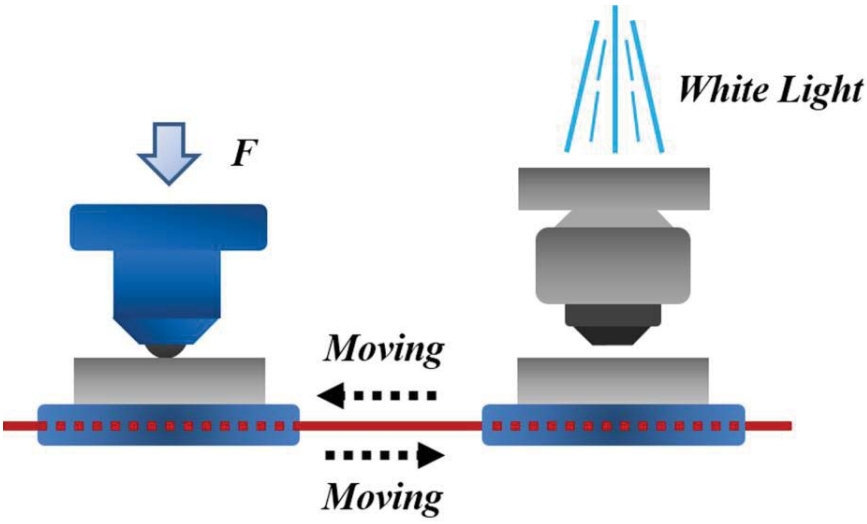

Fig.2 Schematic of the running-in test system (Rtec Tribotester)

Table 1 Operating Parameters in Running-in Process

Parameters	Symbols	Values	Units
Load	*W*	80	N

Average entrainment speeds	U_e	0.08	m/s
Dynamic viscosity of oil (303K)	η_0	0.048	Pa.s
Elastic modulus of material	E	210	GPa
Poisson's ratio	v_1, v_2	0.3	
Density of the oil	ρ_0	850	Kg/m^3

3. Rolling contact micropitting fatigue life predictions

In this section, rolling contact micropitting fatigue lives of all pre and post running-in treated discs were numerically estimated. Working condition for these simulations was set as rolling contact EHL. These are closer to operation conditions of industrial rolling machine components.

According to the rolling contact fatigue theory as mentioned in section 1, fatigue life is correlated to surface pressure distribution, traction stress distribution and subsurface stress distribution, which should be calculated based on the operating conditions. Therefore, details of deterministic EHL and contact mechanics models are introduced in the next section.

3.1 Detailed descriptions of deterministic EHL model

The unified Reynolds equations (1) and (2) could perfectly describe hydrodynamic behavior of oil and direct contact behavior of asperities between rough surfaces [19, 20]. Pressure and film thickness in fluid lubricated regions, where h is larger than δ could be obtained by solving equation (1). While in regions where h is smaller than δ, it was considered that the load is sustained by solids or boundary film. Under this case, equation (2) was employed to calculate contact pressure distributions p_c. In this study, δ was set as 0.1nm. It is easy to find that pressures sustained by solid and fluid could be obtained in the same one iteration step by combining equations (1) and (2), which has more efficient convergence stability as compared to the method when separately calculating two types of pressure distributions [18].

$$\frac{\partial}{\partial x}\left(\frac{\rho}{12\eta}h^3\frac{\partial p_f}{\partial x}\right)+\frac{\partial}{\partial y}\left(\frac{\rho}{12\eta}h^3\frac{\partial p_f}{\partial y}\right)=u\frac{\partial(\rho h)}{\partial x} \tag{1}$$

$$\frac{\partial(\rho h)}{\partial x}=0 \tag{2}$$

In equation (1), film thickness h is expressed as

$$h=h_0+\frac{x^2}{2R_x}+\frac{y^2}{2R_y}+v_e(x,y)+\psi_1(x,y)+\psi_2(x,y) \tag{3}$$

where, h_0 is a rigid gap between the two bodies, $x^2/2R_x + y^2/2R_y$ is geometric profile of the ball, ψ_1 and ψ_2 are surface heights, and v_e is elastic deformation of two bodies. A universal method to calculate $v_e(x, y)$ was introduced by Boussinesq integration [25] as shown in equation (4), which indicates elastic deformation at position (x, y) caused by total pressure $p_f + p_c$ and shear stress f at position (x', y'). Here, a slight difference from the previous studies is that the contribution of frictional shear stress to deformation was also taken into consideration, shown as the second item in the right hand of equation (4) [26].

$$v_e(x,y)=\frac{1}{\pi}\iint_A\left[\frac{2\left[p_f(x',y')+p_c(x',y')\right]}{E\sqrt{(x-x')^2+(y-y')^2}}-f(x',y')\frac{(x-x')}{G\left[(x-x')^2+(y-y')^2\right]}\right]dx'dy' \tag{4}$$

where, E is equivalent elastic modulus, G is equivalent elastic shear modulus. E and G are defined in equation (5) and equation (6). The frictional shear stress is defined in equation (7).

$$E=\left[\frac{1}{2}\left(\frac{1-\nu_1^2}{E_1}+\frac{1-\nu_2^2}{E_2}\right)\right]^{-1} \tag{5}$$

$$G=\left[\frac{1}{2}\left(\frac{(1-\nu_1)(1-2\nu_1)}{E_1}-\frac{(1-\nu_2)(1-2\nu_2)}{E_2}\right)\right]^{-1} \tag{6}$$

$$f(x,y)=\eta(x,y)\dot{\gamma}(x,y)+\mu p_c(x,y) \tag{7}$$

Here, E_1 and E_2 are the Young's moduli of the ball and the disc, ν_1 and ν_2 the Poisson's ratios, $p_c(x, y)$ is the local contact pressure sustained by solids or boundary films, μ is the

comprehensive shear coefficient in boundary lubricated regions and was fixed at 0.15 in this study.

To solve Reynolds equation (1), viscosity-pressure and density-pressure properties were taken into consideration. Descriptions of the physical relations are shown in equations (8) and (9).

$$\eta = \exp\left\{\left(\ln\eta_0 + 9.67\right)\left[\left(1+5.1\times10^{-9}\,p_f\right)^{-1.1}-1\right]\right\} \tag{8}$$

$$\rho = \rho_0\left(1+\frac{0.6\times10^{-9}\,p_f}{1+1.7\times10^{-9}\,p_f}\right) \tag{9}$$

Because oil exhibits shear shinning phenomenon under high shear rate, non-Newtonian property of the lubricant was described by introducing Bair and Winner's rheology model [27].

$$\dot{\gamma}(x,y) = -\frac{\tau_L}{\eta(x,y)}\ln\left(1-\frac{\tau(x,y)}{\tau_L}\right) \tag{10}$$

where τ_L is a characteristic shear stress of the lubricant, set as 18MPa in the simulation, which is a typical value for mineral oils [9].

3.2 Rolling contact fatigue life prediction model

In the numerical estimations of contact fatigue lives, Zaretsky model was adopted since it could adequately correlate the freewill stress distributions in subsurface and load cycles before fatigue cracks initiate [6]. The mathematical form of this model is shown in formula (11).

$$\ln\frac{1}{S} = AN^e\iiint_V {\tau_{vM}}^{ec}(x,y,z)\,dV \tag{11}$$

where, τ_{vM} is equivalent von Mises stress in the subsurface of the contact body, V is stress volume, S is survival probability of material before N stress cycles, e is Weibull slope and c is stress index. A is a coefficient set as 1×10^{-10}, which is related to materials [28].

3.3 Subsurface contact stress field calculation method

To obtain τ_{vM} in equation (11), stress field in subsurface under distributed pressure should be calculated aforehand. Most accepted method to calculate contact stress is to assume that contacting bodies are semi-infinite [29]. When normal pressure p and traction stress f applied on a solid surface, stress components at position (x, y, z) within subsurface could be calculated as formula (12) [29].

$$\begin{aligned}\sigma_{mn}(X,Y,Z) = &\iint_{\Omega} G_{p,mn}(X-\zeta,Y-\xi,Z)\,p(\zeta,\eta)\,d\zeta\,d\xi \\ &+\iint_{\Omega} G_{f,mn}(X-\zeta,Y-\xi,Z)\,f(\zeta,\eta)\,d\zeta\,d\xi\end{aligned} \tag{12}$$

where, G_p and G_f are Green functions [30], ζ and ξ are Cartesian coordinates in the calculation region. Values of subscripts m and n can only be equal to 1 or 2 or 3, which represent three directions of stress component.

The integration in equation (12) can be rewritten into discrete form as equation (13)[30], which are convolutions of p and D_p, f and D_f.

$$\begin{aligned}\sigma_{mn}(X_i,Y_j,Z_k) = &\sum\sum p(\zeta_q,\xi_l)\,D_{p,mn}(X_i-\zeta_q,Y_j-\xi_l,Z_k) \\ &+\sum\sum f(\zeta_q,\xi_l)\,D_{f,mn}(X_i-\zeta_q,Y_j-\xi_l,Z_k)\end{aligned} \tag{13}$$

where, D_p and D_f indicate influence coefficients. Detailed expressions of D_p and D_f are shown in appendix A. Subscripts i, j, k, q and l indicate discrete counting variables.

It could be easily found that computation of equation (13) is extremely time consuming. Therefore, DC-FFT method is applied to improve the speed of convolution [30]. After the all stress components within subsurface were obtained, equivalent stress τ_{vm} could be determined by the following expression [31].

$$\begin{aligned}\tau_{vm}(X_i,Y_j,Z_k) = \frac{1}{\sqrt{2}}\Big\{&\left[\sigma_{11}(X_i,Y_j,Z_k)-\sigma_{22}(X_i,Y_j,Z_k)\right]^2 \\ &+\left[\sigma_{11}(X_i,Y_j,Z_k)-\sigma_{33}(X_i,Y_j,Z_k)\right]^2 \\ &+\left[\sigma_{22}(X_i,Y_j,Z_k)-\sigma_{33}(X_i,Y_j,Z_k)\right]^2 \\ &+6\left[\sigma_{12}(X_i,Y_j,Z_k)+\sigma_{13}(X_i,Y_j,Z_k)+\sigma_{23}(X_i,Y_j,Z_k)\right]^2\Big\}^{0.5}\end{aligned} \tag{14}$$

4 Results

4.1 Morphological feature during running-in process

To study the effects of various morphologies on rolling contact fatigue life, experimental running-in methods have been introduced to form different rough surfaces. Detailed procedures and operating parameters have been described in section 2.1.

Figure 3 displays surface height, root mean square roughness (R_q) and comparisons of the rubbed regions pre and post running-in process. It can be seen from figure3 (a) and (b) in each case that there are obvious reductions of surface heights in the wear region after running-in. However, original grooves which formed on surface finishing still existed, which indicates mild wear mainly occurred during running-in. This is because of high asperities were removed continually during friction process while other lower regions were protected by oil film or boundary film under mixed lubrication. It can also be seen that the R_q visibly decreases in the rubbed regions for all post running-in cases. This has been attributed to high asperities of the original surfaces which were worn off while low regions remained unchanged on the surfaces. In figure 3, there are some long sliding grooves appearing on the surface after running-in tests such as case 1, case 4 and case 5. It is most probably because adhesive wear occurred and some hard particles remained adhered to the ball which had been scratching the surface of the disc.

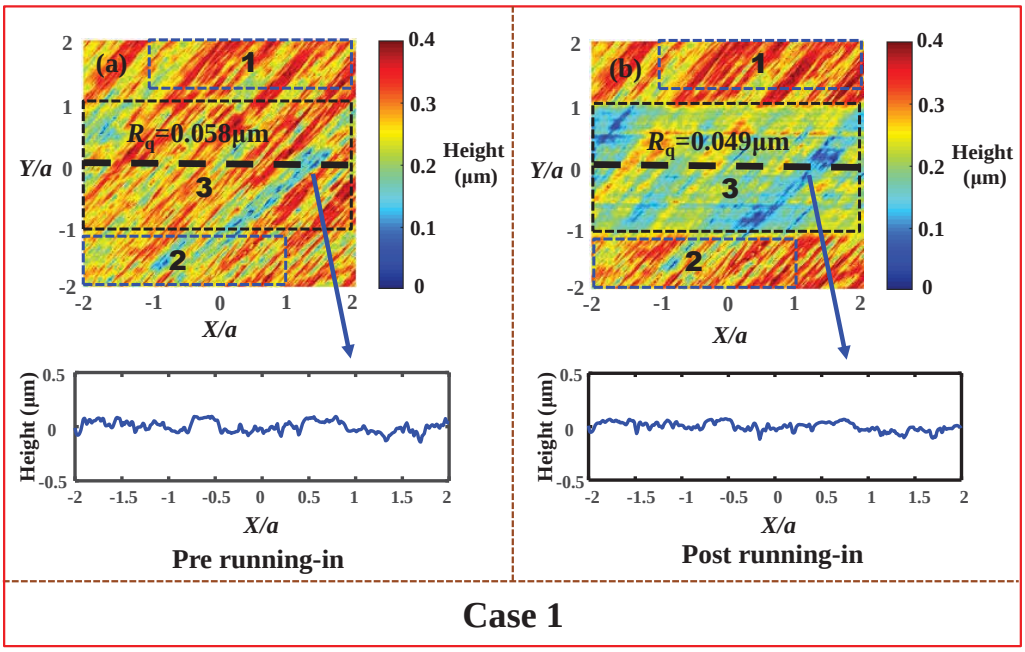
(a)
(b)
1
2
3
R_q=0.058μm
R_q=0.049μm
Y/a
X/a
Height (μm)
Pre running-in
Post running-in
Case 1

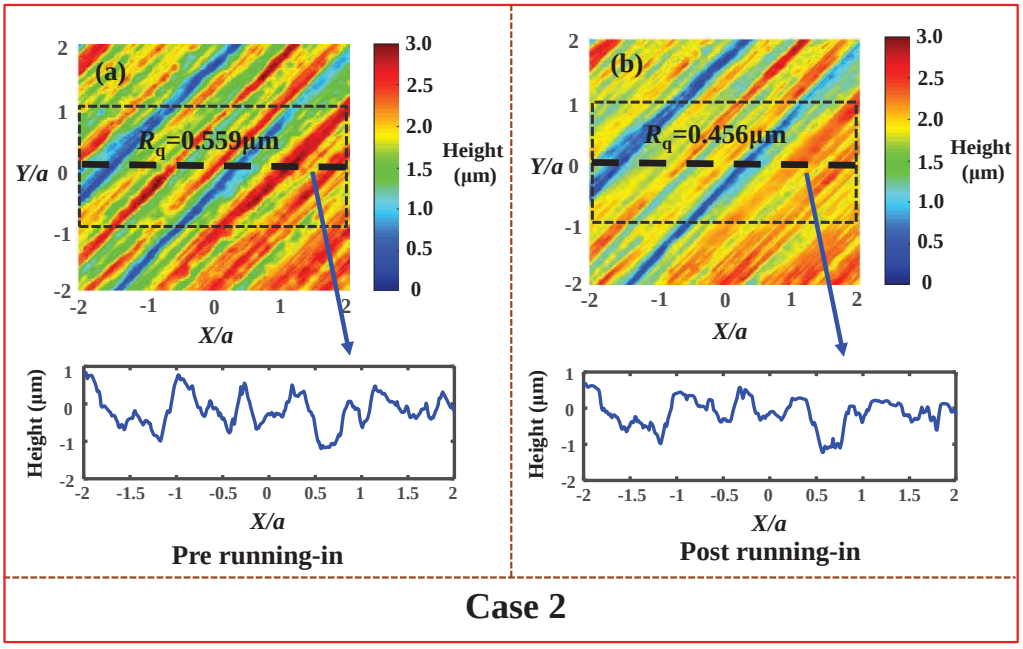
(a)
(b)
R_q=0.559μm
R_q=0.456μm
Y/a
X/a
Height (μm)
Pre running-in
Post running-in
Case 2

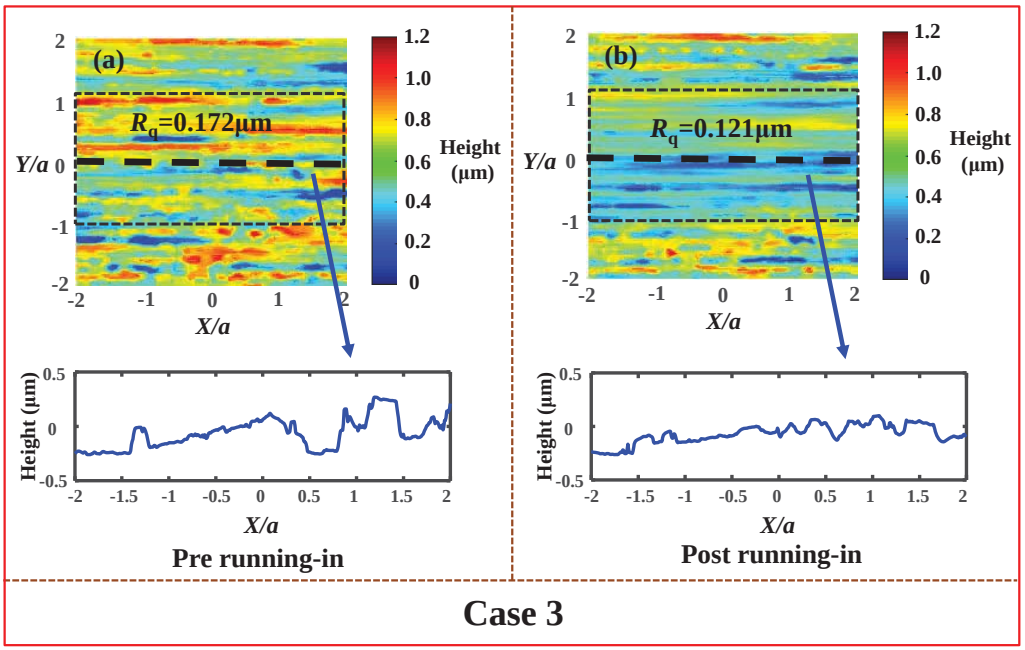
(a)
R_q=0.172μm
(b)
R_q=0.121μm
Height (μm)
Y/a
X/a
Pre running-in
Post running-in
Case 3

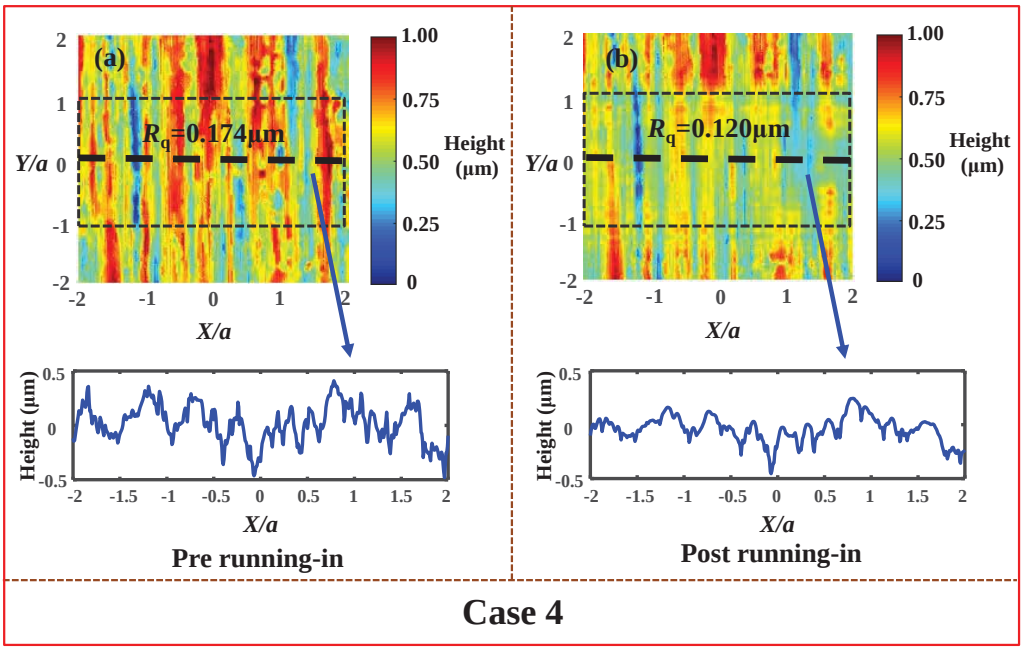
(a)
R_q=0.174μm
(b)
R_q=0.120μm
Height (μm)
Y/a
X/a
Pre running-in
Post running-in
Case 4

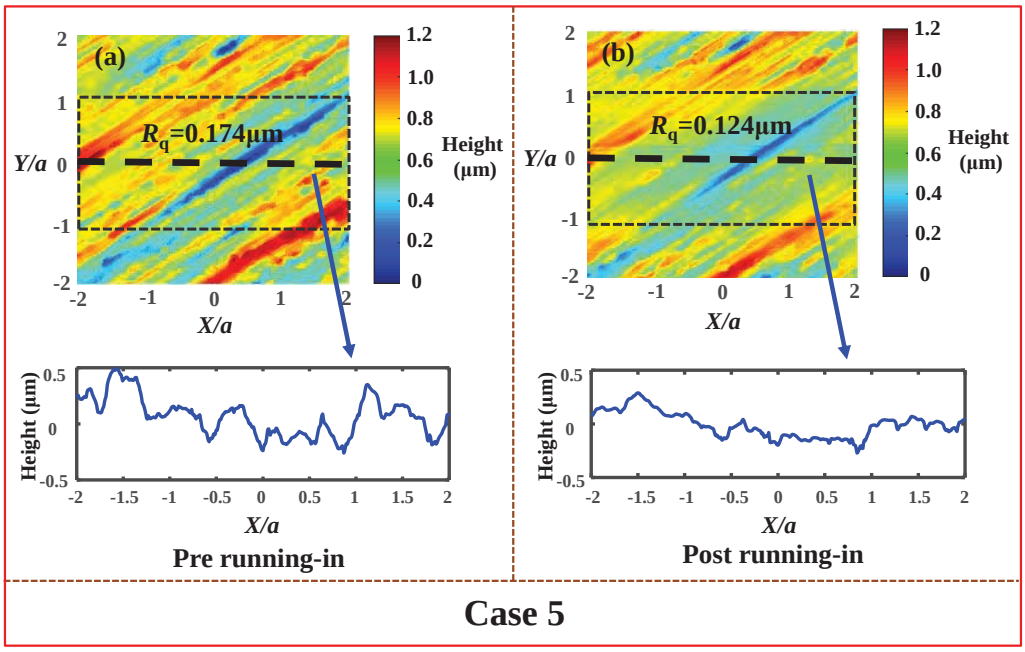

Fig. 3 Comparisons of morphology of wear regions pre and post running-in for the test cases

4.2 Validation of models

In this section, deterministic EHL model calculation methods and von Mises stress are validated. Figure 4 shows comparison of smooth EHL solutions of previous and present studies under the same operating conditions. It could be seen they correspond well with each other. Figure 5 shows von Mises stress field of smooth contact case calculated by using equation (12) through to equation (14). In this calculation, shear stress was taken into consideration by setting a dry friction coefficient of 0.25. It could be seen that the results of present study shows good agreement with [32].

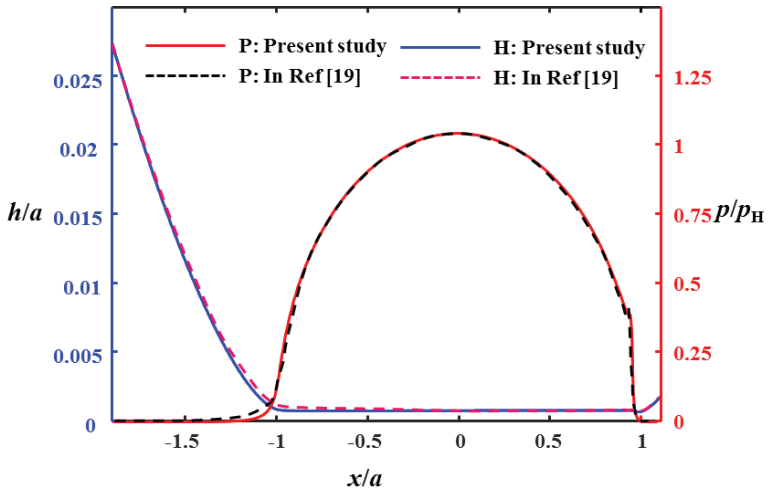

Fig. 4 Comparison of Smooth EHL solutions between present study and [19]: U = 0.625m/s, W^* = 1.008×10^{-5}, G^* = 4000;

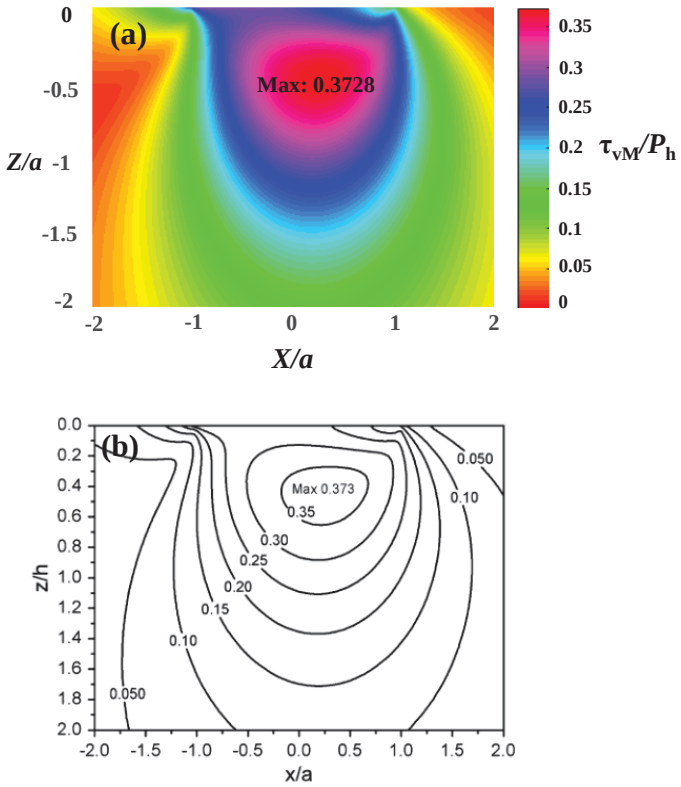

Fig. 5 Von Mises stress in the subsurface: normal load F_N = 100N, shear coefficient f_s = 0.25, results of previous study [32]. (a) Results of present study. (b) Results in [32].

4.3 Estimations of rolling contact micropitting fatigue lives

As described in section 1, the spalling failures mainly depend on the total contact load and material's mechanical properties. Hence, topography modification has little effect on changing the spalling fatigue lives. However, micropitting fatigue has close relation with the detailed pressure distributions, which indicates the microstructure of surface topography can affect the micropitting fatigue lives. Therefore, in this study, attention was focused on the effect of different surface characteristic on the rolling contact micropitting fatigue lives. Here, rolling contact micropitting fatigue lives of all the surfaces pre and post running-in under lubricated conditions were numerically estimated and compared based on equation (11). For each case, the depths range of micropitting and spalling fatigues are fixed at 20μm and 150μm, respectively. In order to compare the effect of running-in on fatigue lives, two index are defined and their physical meanings are given as follow.

1. The relative fatigue life (*RFL*) is obtained by dividing real rough surface rolling contact fatigue life by smooth surface rolling contact fatigue life, and this is expressed by the following formula (15).

$$RFL = \frac{L_{real}}{L_{smooth}} \tag{15}$$

where, L_{real} indicates rolling contact fatigue life of rough surfaces under the operating condition shown in Table 2, L_{smooth} is the rolling contact fatigue life of an ideal smooth surface.

2. The improvement rate of fatigue life (*IRFL*) was calculated by formula (16).

$$IRFL = \frac{L_r - L_o}{L_o} \times 100\% \tag{16}$$

where, L_r means the rolling contact fatigue life of post running-in surface, L_o means the fatigue life of pre running-in surface.

Table 2. Simulation parameters in fatigue life calculations

Parameters	Symbols	Values	Units
Load	*W*	80	N

Entrainment speeds	U_e	0.5	m/s
Sliding to rolling ratio	s	0.5	
Computation domain of X		$-2a \le X \le 2a$	
Computation domain of Y		$-2a \le Y \le 2a$	
Weibull slope	e	1.11	
Stress index	c	9.1	
Survival reliability	S	0.9	
Hertz contact radius	a	Determined by material and W	m

Figure 6 shows rolling contact fatigue lives of the five discs pre and post a running-in process subject to operating conditions as shown in Table 2. Here the operating conditions are different from that in the running-in because the above running-in process was conducted for the purpose to change the original surface topography. In other words, the surfaces with and without the running-in only provide different input topographies information for comparing the fatigue lives. It could be seen from figure 6 (a) that rolling contact micropitting fatigue lives could be significantly improved after the running-in process and it is conveyed more explicitly by using *IRFL* in figure 7. However, spalling contact fatigue life shown in figure 6 (b) and figure 7, changes inappreciable comparing with micropitting fatigue life. It is because spalling fatigue forms in deep subsurface, where stress field is determined by Hertz pressure and surface microstructure does not have significant influence on it.

In figure 6, the fatigue life in case 1 is higher than the other cases whether it is pre or post running-in process. This is due to the original surface of case 1, which has relatively the lowest roughness among all the cases, which results in the lowest subsurface stress in case 1 near the surface. Correspondingly, the relative fatigue life of case 2 is shortest because of the largest surface roughness. However, *IRFL* in case 3 is prominent in figure 7 while that of in case 1 is not very significant. This is because that the surface roughness modification of relative smooth surface is limited while that of rough surface is more conspicuous.

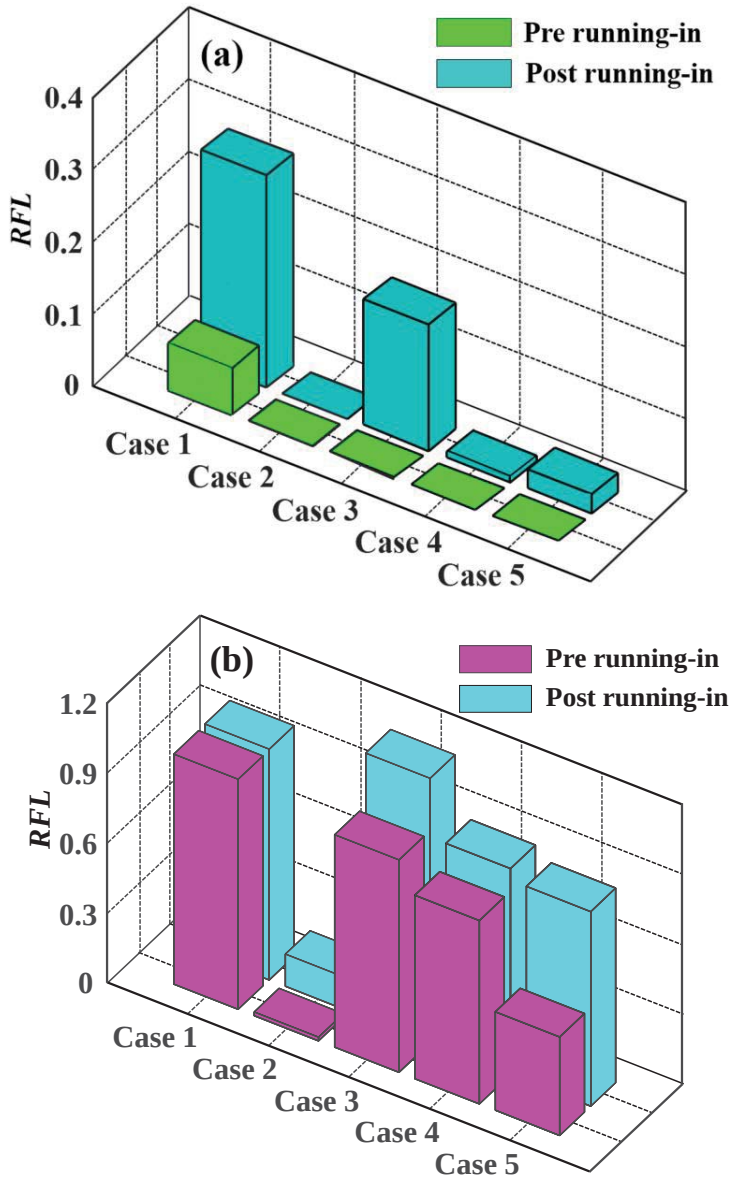

Fig. 6 Comparisons of relative rolling contact fatigue lives pre and post running-in process (a) relative micropitting fatigue lives. (b) relative spalling fatigue lives.

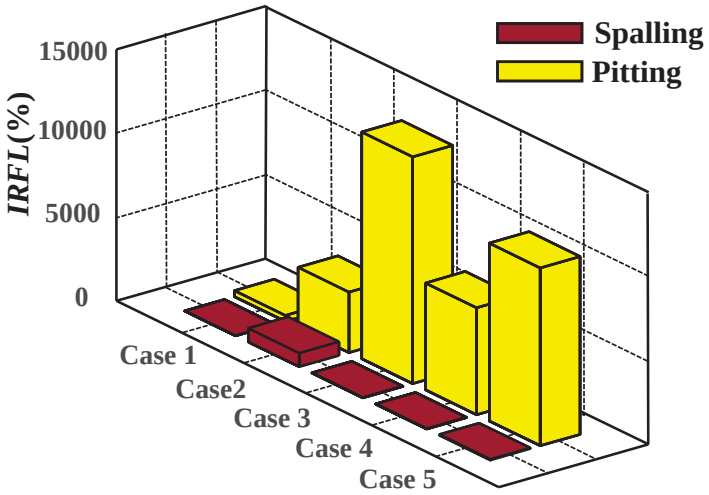

Fig. 7 *IRFL* (%) of the five discs under EHL lubricated condition of rolling contact

5 Discussions

5.1 Implications of varying surface topographies on subsurface stress fields

It could be concluded that rolling contact fatigue life is enhanced due to decreased von Mises stress in the subsurface as evident from equation (11). Therefore, in this section, the lubrication and contact behaviors of the tribo-pair under the same operating conditions as Table 2 were simulated. These simulations were performed to demonstrate that how running-in has an influence on rolling fatigue lives.

Figure 8 shows a comparison between pressure distributions and von Mises stress fields in all cases pre and post running-in. It could be seen, after disc running-in, that both the pressure fluctuations on the surface and the stress fluctuations within the subsurface decrease. Based on these results, it is theoretically proved that micro pitting fatigue life is improved due to the stress decrease in shallow depths of subsurface after running-in. Additionally, it could be found that the variations of pressure and von Mises stress in case 1 is less obvious than that of case 2. A similar behavior is demonstrated in figure 8, where the *IRFL* in case 1 is much smaller than in case 2. Figure 8 also shows that variations of stress are less intense in relative deep positions of subsurface after running-in, which

theoretically explains as to why the spalling fatigue life is mainly determined by the Hertz pressure rather than infinitesimal pressures.

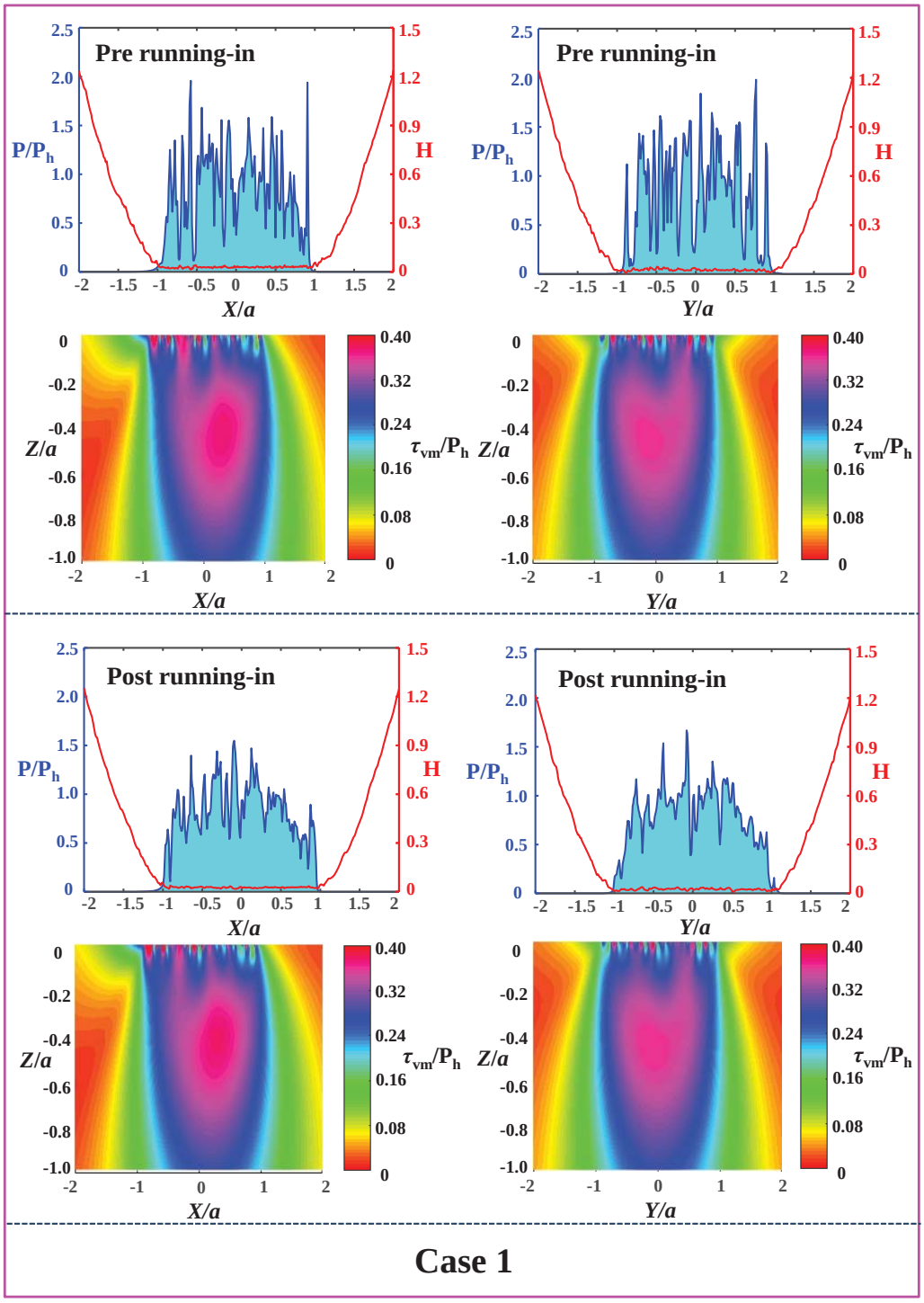

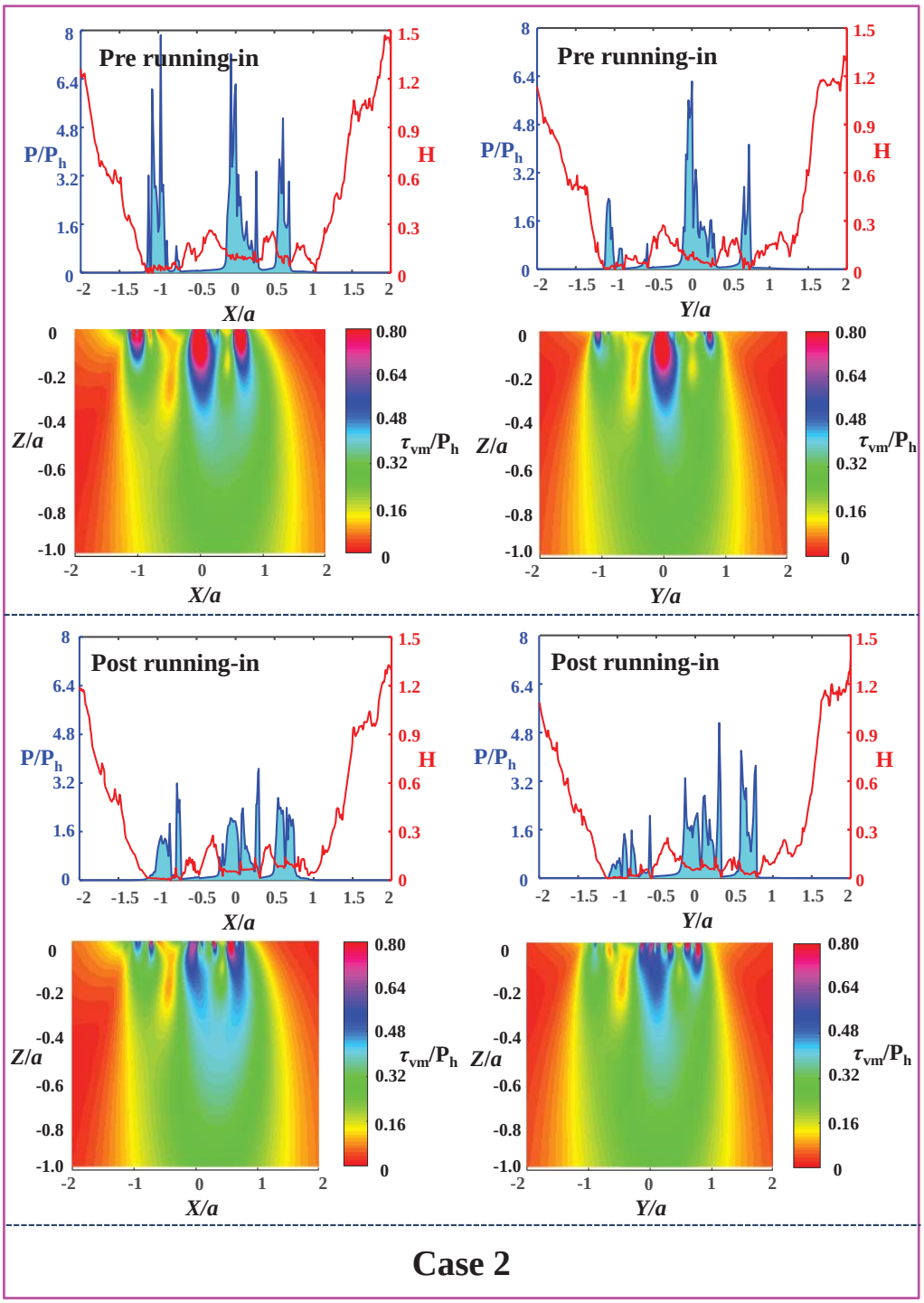
Pre running-in
Pre running-in
Post running-in
Post running-in
P/P_h
H
X/a
Y/a
Z/a
τ_vm/P_h
Case 2

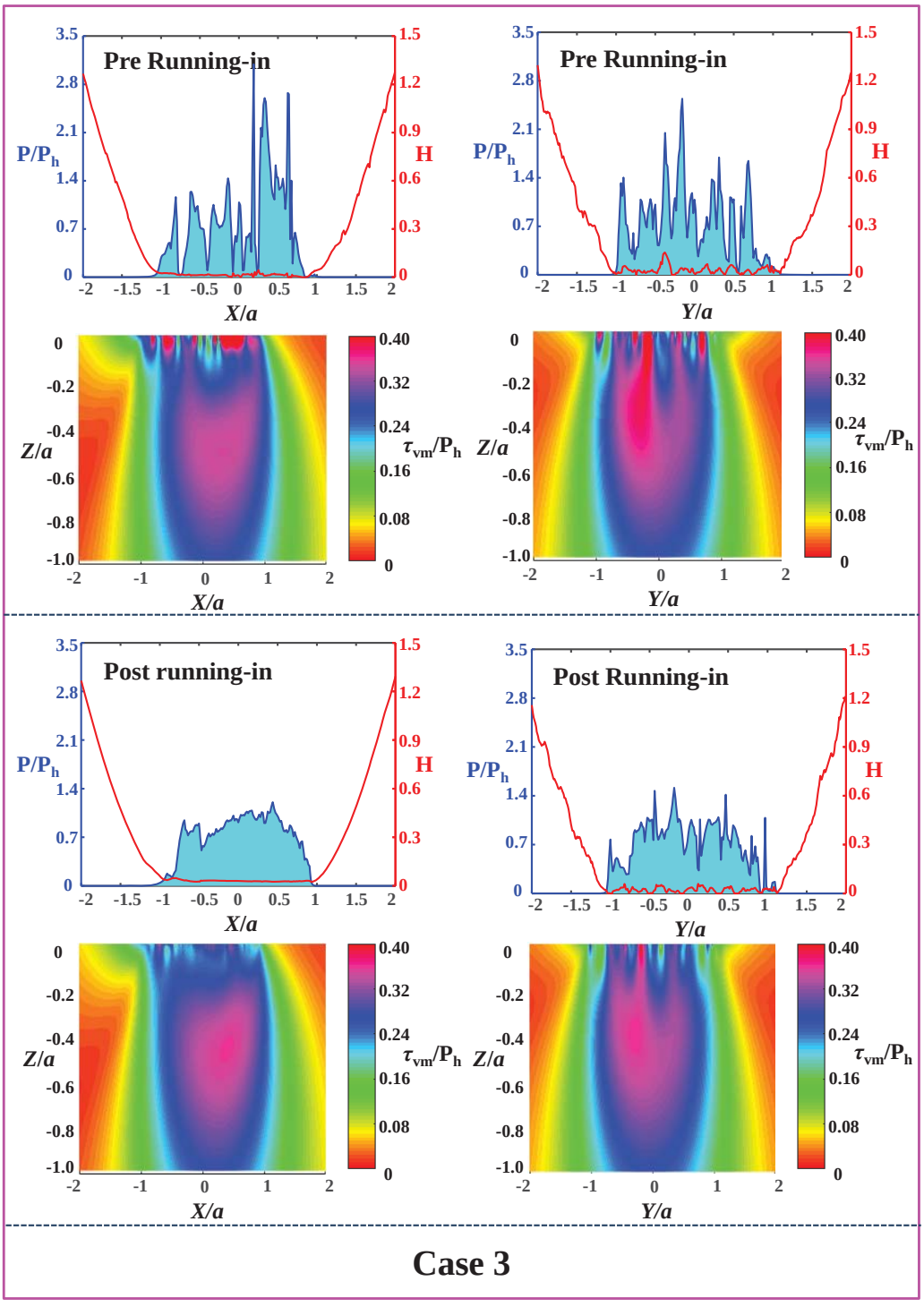
Pre Running-in
P/P_h
H
X/a
Z/a
τ_vm/P_h
Pre Running-in
Y/a
Post running-in
Post Running-in
Case 3

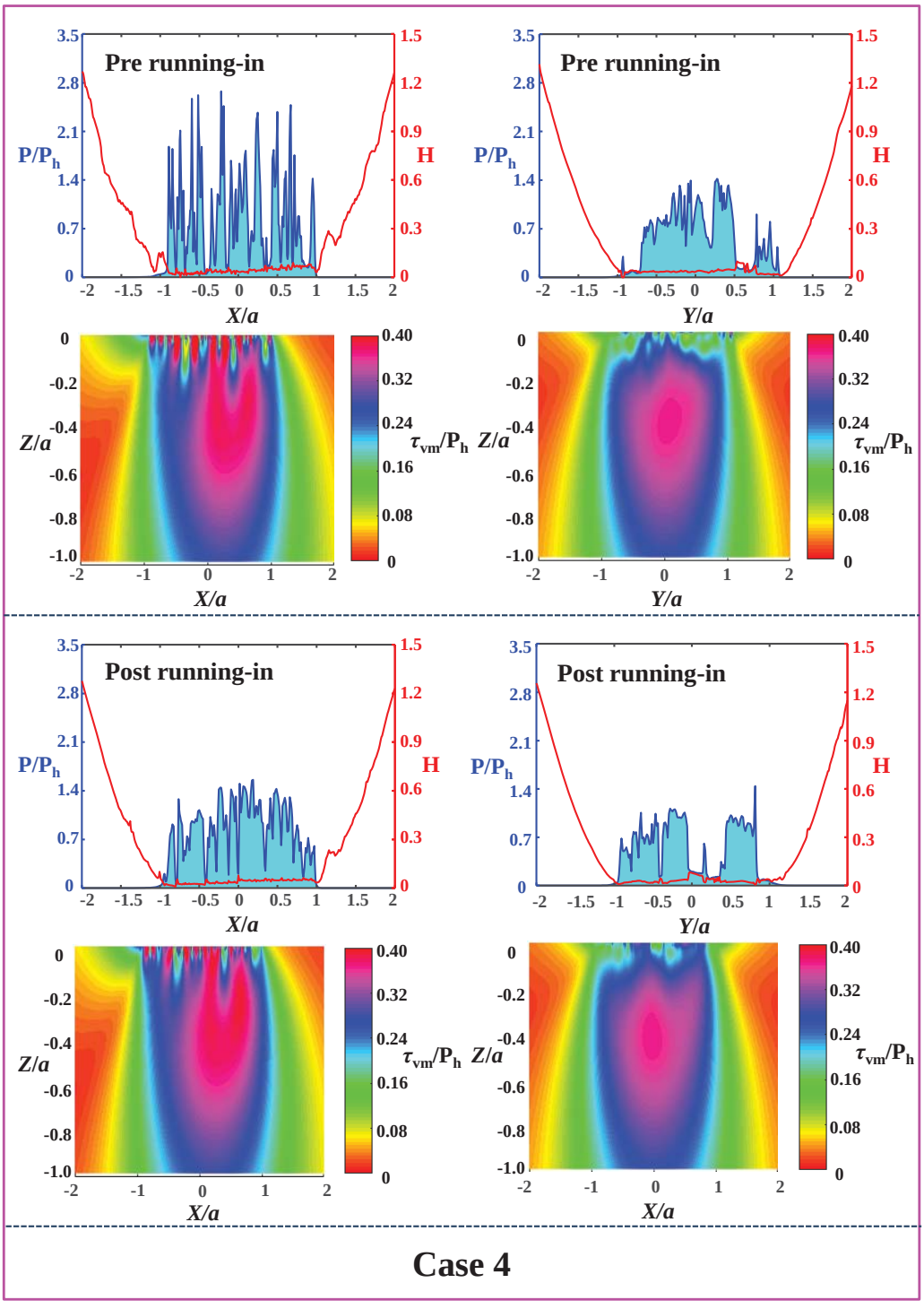
Pre running-in
P/P_h
H
X/a
Pre running-in
P/P_h
H
Y/a
Z/a
τ_vm/P_h
X/a
Z/a
τ_vm/P_h
Y/a
Post running-in
P/P_h
H
X/a
Post running-in
P/P_h
H
Y/a
Z/a
τ_vm/P_h
X/a
Z/a
τ_vm/P_h
X/a
Case 4

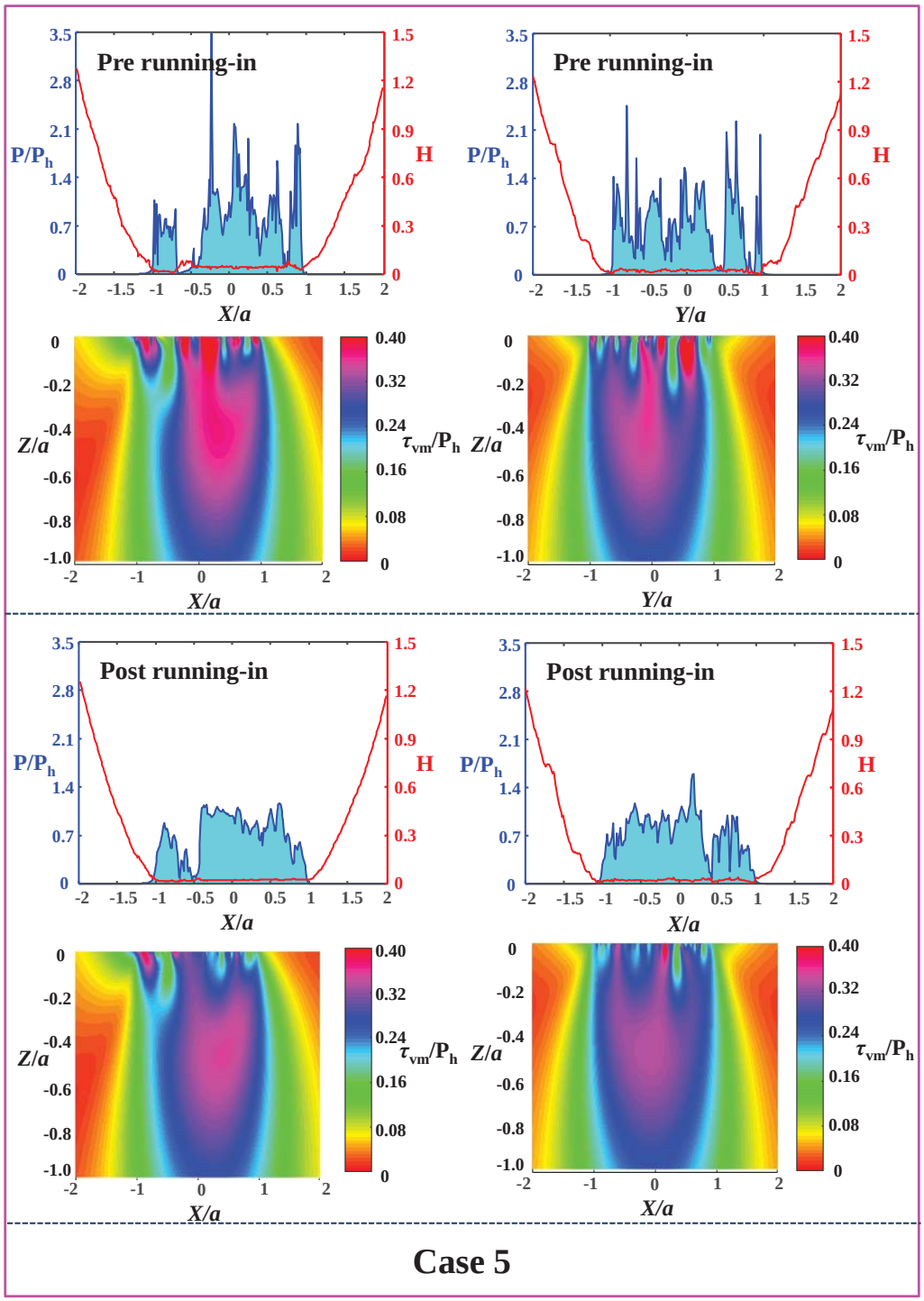

Fig. 8 Comparisons of contact behaviors between surfaces pre and post a running-in under rolling EHL condition

5.2 Effects of surface topographical characteristics on rolling contact micropitting fatigue lives

Summarizing the above results, it can be concluded that micropitting fatigue life was modified after running-in due to the original surface being smoothen. The R_q in the contact regions pre and post running-in were plotted in figure 9. There are slight differences of R_q values as compared with figure 3 since the R_q in figure 9 only indicates the circular contact region while in figure 3 it indicates the whole wear scar. It could be seen that the R_q decreases in all cases after running-in, which is a supposed reason for modifying micropitting fatigue life after running-in. However, for a general rough surface, smaller R_q is not the only factor that results in longer micropitting fatigue lives, which could be demonstrated by comparing case 1 and case 3 in figure 6 and figure 9. It could be seen that the micropitting fatigue life in case 3 after running-in is higher than that of case 1 before running-in while their R_q values present inverse trend (the R_q in case 3 post running-in is higher than that of case 1 pre running-in). We can also see that the R_q values of case 3, case 4 and case 5 are very similar both pre and post running-in, but the micropitting fatigue lives of these surfaces are distinctly different. This phenomenon indicates that the R_q (or the film thickness ratio λ in other words) is not the exclusive topography factor which determines rolling contact micropitting fatigue lives.

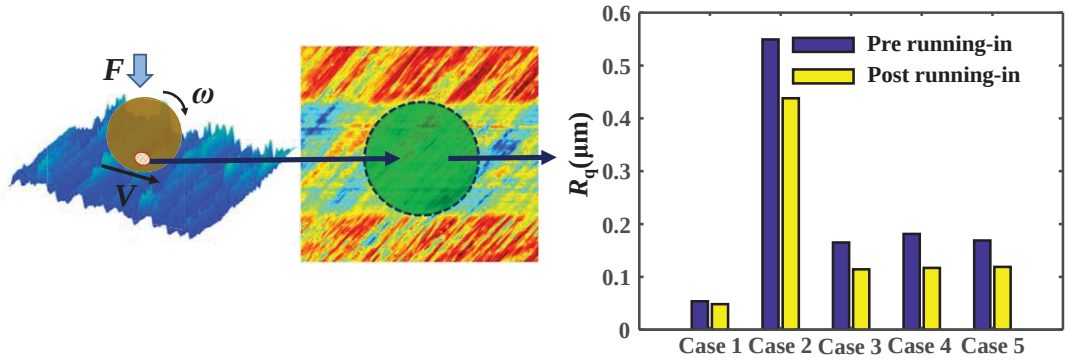

Fig.9 Comparisons of R_q values of surfaces pre and post a running-in process within the contact region

When asperity radius is large, grain steepness on surface is gradual, which results in smoother distribution of pressure. If the asperity radius is small, the pressure oscillates vigorously, which in turn causes large fluctuations of von Mises stress in the subsurface.

It is therefore desirable to investigate whether different asperity radius results in different micropitting fatigue lives and what is the relationship between the two. Based on the above questions, mean asperity radius values of the contact regions for all the cases were calculated and summarized in figure 10. Calculation method of asperity radius is similar to that in [33]. Each asperity was identified by using the 8 points method [33], which assumes that the height of an asperity is higher than the neighboring 8 points. After the positions of all the asperities within contact region were found out, their radii were calculated by the method given in appendix B. Mean asperity radius is the arithmetic mean value of all the asperity radii.

It could be seen that mean asperity radius, r_s, increases significantly after running-in but the increments are different. Combining figure 6 and figure 10, it could also be found that larger r_s corresponds to higher micropitting fatigue lives and vice-versa. This indicates the mean asperity radius of rough surface is also a factor that influences the micropitting fatigue lives. However, similar to R_q, mean asperity radius is not the single factor affecting the micropitting fatigue. This can be proved by comparing the results of case 1 and case 5. In figure 10, the r_s in case 5 post running-in is larger than that of case 1 irrespective of pre or post running-in, on the other hand the trend of their micropitting fatigue lives are inverse as shown in figure 6. Therefore, it is assumed here that the micropitting fatigue life is influenced by the combined effect of R_q and r_s.

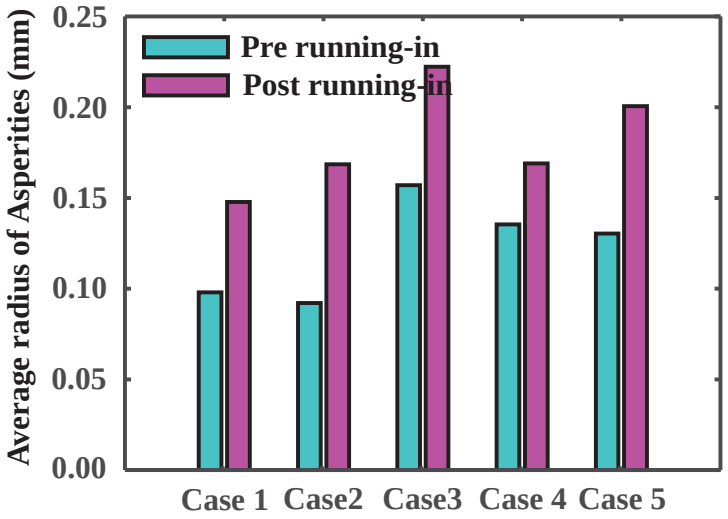

Fig.10 Comparisons of mean asperity radius of surfaces pre and post running-in process within the contact region

In order to validate the above assumption, the relation between the micropitting fatigue life and R_q/r_s was fully investigated.

Here, the R_q/r_s is proposed as a new statistical parameter of rough surface that mainly affects the micropitting fatigue lives. Compared with the plastic index, R_q/r_s does not contain elastic modulus and hardness because rolling contact fatigue cracks mostly propagate under elastic range. Hence it has not been taken into consideration in R_q/r_s parameter. The relationship between relative micropitting fatigue lives and R_q/r_s is shown in figure 11.

It could be seen that relative micropitting fatigue lives reduce rapidly with an increase in R_q/r_s, which indicates that there is an obvious reduction of pressure fluctuations and von Mises stress near the surface with a decrease of R_q and an increase of r_s. The fast decrease of relative fatigue life is due to the load cycles N in equation (11) is inversely proportional to 9.1 times power of the von Mises stress. The effect of R_q/r_s on von Mises stress could be seen by comparing case 3, case 4 in figure 8 and figure 10. In figure 10, the surface in case 3 post running-in has a similar R_q but larger r_s compared with case 4 post running-in and correspondingly the stress fluctuations is much smaller in the former than the latter as shown in figure 8. In other words the smaller R_q/r_s could result in smaller von Mises stress. Therefore, in summary of the above analyses, there is a clear negative correlation between R_q/r_s and micropitting fatigue lives.

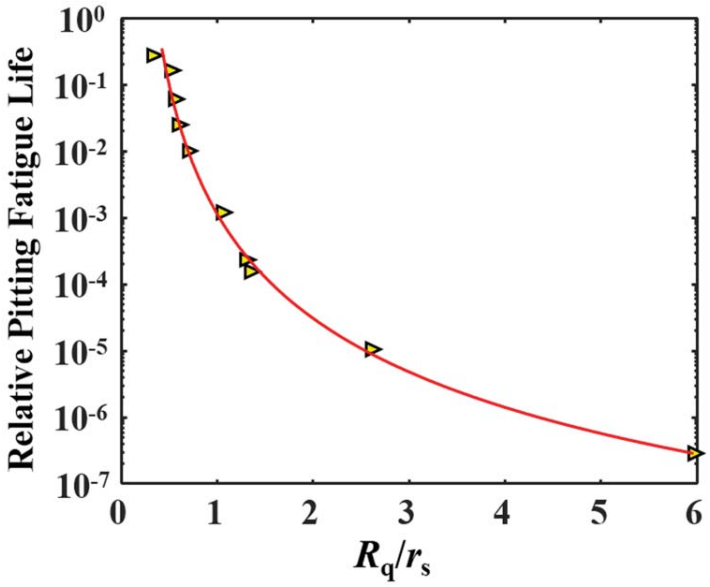

Fig.11 Relative micropitting fatigue lives vs R_q/r_s for all the rough surfaces

6 Conclusions

Rolling contact micro pitting fatigue lives subject to EHL condition were numerically estimated based on a series of rough surfaces pre and post running-in treatment. Meanwhile, the morphology was statistically analyzed to study how the topographical parameters affect the fatigue lives. The following key conclusions can be drawn from this study;

1. For a rough surface, the rolling contact fatigue life can be improved by subjecting it to a certain running-in process.
2. The improvement of micropitting fatigue life by running-in is usually constraint up to 0.4 as after running-in the surface is not ideally smooth.
3. From statistical aspects, small surface R_q and a large asperity radius r_s, has benefits in terms of reducing micropitting fatigue failures.
4. Micropitting fatigue life was affected by the aggregate effects of R_q and r_s rather individually. A decrease in R_q/r_s has a positive effect on enhancing micropitting fatigue lives.

Acknowledgment

The authors would like to acknowledge the Ministry of Industry and Information Technology, China, with grant number JSZL2017213B002 and the National Natural Science Foundation of China (NSFC) for providing financial support with grant number 51635009 to conduct this research.

Appendix A

Detailed expression of influent coefficient D is shown as follow [33].

$$D_{p,mn}(X,Y,Z)=\left[G_{p,mn}(X_{-},Y_{-},Z)+G_{p,mn}(X_{+},Y_{+},Z)+G_{p,mn}(X_{-},Y_{+},Z)+G_{p,mn}(X_{+},Y_{-},Z)\right] \tag{A.1}$$

$$D_{f,mn}(X,Y,Z)=\left[G_{f,mn}(X_{-},Y_{-},Z)+G_{f,mn}(X_{+},Y_{+},Z)+G_{f,mn}(X_{-},Y_{+},Z)+G_{f,mn}(X_{+},Y_{-},Z)\right] \tag{A.2}$$

Where, m and n equal 1, 2 and 3, G is the integration of Green function, the expression of which is shown from equation (A.3) to equation (A.14), the $X_{-}=X-0.5\Delta X$, $X_{+}=X+0.5\Delta X$, $Y_{-}=Y-0.5\Delta Y$ and $Y_{+}=0.5\Delta Y$.

$$G_{p,11}(x,y,z)=\frac{1}{2\pi}\left[(2-4\nu)\tan^{-1}\left(\frac{x}{\sqrt{x^2+y^2+z^2}+y+z}\right)-2\nu\tan^{-1}\left(\frac{xy}{z\sqrt{x^2+y^2+z^2}}\right)-\frac{xz}{\sqrt{x^2+y^2+z^2}\left(\sqrt{x^2+y^2+z^2}+y\right)}\right] \tag{A.3}$$

$$G_{p,22}(x,y,z)=\frac{1}{2\pi}\left[(2-4\nu)\tan^{-1}\left(\frac{y}{\sqrt{x^2+y^2+z^2}+y+z}\right)-2\nu\tan^{-1}\left(\frac{xy}{z\sqrt{x^2+y^2+z^2}}\right)-\frac{yz}{\sqrt{x^2+y^2+z^2}\left(\sqrt{x^2+y^2+z^2}+x\right)}\right] \tag{A.4}$$

$$G_{p,33}(x,y,z)=\frac{1}{2\pi}\left[-\tan^{-1}\left(\frac{xy}{z\sqrt{x^2+y^2+z^2}}\right)+\frac{xz}{\sqrt{x^2+y^2+z^2}\left(\sqrt{x^2+y^2+z^2}+x\right)}+\frac{yz}{\sqrt{x^2+y^2+z^2}\left(\sqrt{x^2+y^2+z^2}+y\right)}\right] \tag{A.5}$$

$$G_{p,12}(x,y,z)=\frac{1}{2\pi}\left[(2\nu-1)\ln\left(\sqrt{x^2+y^2+z^2}+z\right)-\frac{z}{\sqrt{x^2+y^2+z^2}}\right] \tag{A.6}$$

$$G_{p,13}=\frac{1}{2\pi}\frac{-z^2}{\sqrt{x^2+y^2+z^2}\left(\sqrt{x^2+y^2+z^2}+y\right)} \tag{A.7}$$

$$G_{p,23}=\frac{1}{2\pi}\frac{-z^2}{\sqrt{x^2+y^2+z^2}\left(\sqrt{x^2+y^2+z^2}+x\right)} \tag{A.8}$$

$$G_{f,11}(x,y,z)=\frac{1}{2\pi}\left\{2\ln\left(\sqrt{x^2+y^2+z^2}+y\right)-\frac{2\nu x^2}{\sqrt{x^2+y^2+z^2}\left(\sqrt{x^2+y^2+z^2}+y\right)}+z(1-2\nu)\left[\frac{y}{\sqrt{x^2+y^2+z^2}\left(\sqrt{x^2+y^2+z^2}+z\right)}+\frac{z}{\sqrt{x^2+y^2+z^2}\left(\sqrt{x^2+y^2+z^2}+y\right)}\right]\right\} \tag{A.9}$$

$$G_{f,22}(x,y,z)=\frac{1}{2\pi}\left[2\nu\ln\left(\sqrt{x^2+y^2+z^2}+y\right)-\frac{2\nu y}{\sqrt{x^2+y^2+z^2}}-z(1-2\nu)\left(\frac{y}{\sqrt{x^2+y^2+z^2}\left(\sqrt{x^2+y^2+z^2}+z\right)}\right)\right] \tag{A.10}$$

$$G_{f,33}(x,y,z)=\frac{1}{2\pi}\left[\frac{-z^2}{\sqrt{x^2+y^2+z^2}\left(\sqrt{x^2+y^2+z^2}+y\right)}\right] \tag{A.11}$$

$$G_{f,12}(x,y,z)=\frac{1}{2\pi}\left[\ln\left(\sqrt{x^2+y^2+z^2}+x\right)-\frac{2\nu x}{\sqrt{x^2+y^2+z^2}}\right.$$
$$\left.-z(1-2\nu)\left(\frac{x}{\sqrt{x^2+y^2+z^2}\left(\sqrt{x^2+y^2+z^2}+z\right)}\right)\right] \tag{A.12}$$

$$G_{f,13}(x,y,z)=\frac{1}{2\pi}\left[\frac{-xz}{\sqrt{x^2+y^2+z^2}\left(\sqrt{x^2+y^2+z^2}+y\right)}-\tan^{-1}\left(\frac{xy}{z\sqrt{x^2+y^2+z^2}}\right)\right] \tag{A.13}$$

$$G_{f,23}(x,y,z)=\frac{1}{2\pi}\frac{-z}{\sqrt{x^2+y^2+z^2}} \tag{A.14}$$

Where, v is the Poisson's ratio of material.

Appendix B

On a general rough surface, schematic of an asperity radius is shown in Fig B1. Curvatures of an asperity in x and y directions are usually not equal. Therefore, the equivalent curvatures of the asperity is

$$K=\sum K_I=K_x+K_y \tag{B.1}$$

Where, K_I indicates the curvature in one direction of an asperity. The expression of K_I is

$$K_I=\frac{\left|\frac{d^2z}{dx^2}\right|}{\left(1+\left(\frac{dz}{dx}\right)^2\right)^{\frac{3}{2}}} \tag{B.2}$$

Where, z is the height of asperity on rough surface.

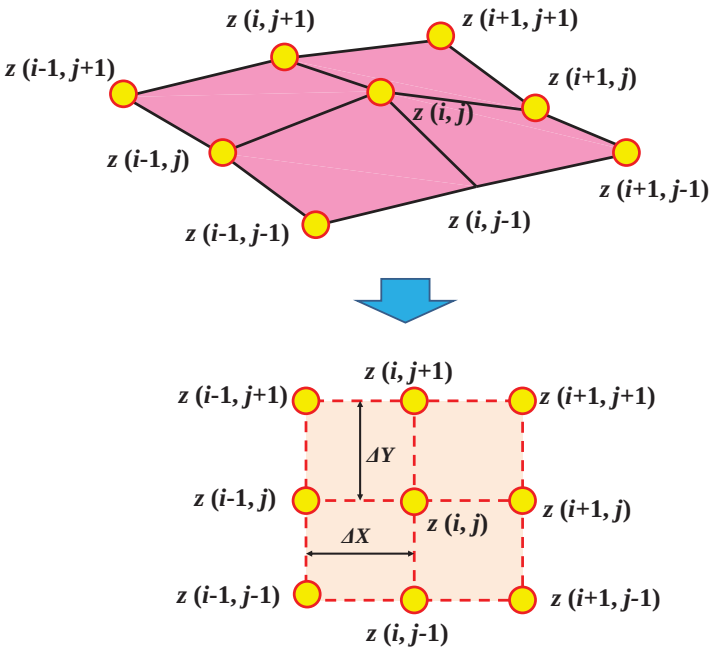

Figure B1. Schematic of an asperity radius

Since the height of a rough surface is discrete in real measurement, the equivalent curvature K was calculated in discretization scheme as

$$K = \frac{\frac{z_{i+1,j} - 2z_{i,j} + z_{i-1,j}}{\Delta X^2}}{\left(1 + \left(\frac{z_{i+1,j} - 2z_{i,j} + z_{i-1,j}}{2\Delta X}\right)^2\right)^{\frac{3}{2}}} + \frac{\frac{z_{i,j+1} - 2z_{i,j} + z_{i,j-1}}{\Delta Y^2}}{\left(1 + \left(\frac{z_{i,j+1} - 2z_{i,j} + z_{i,j-1}}{2\Delta Y}\right)^2\right)^{\frac{3}{2}}} \tag{B.3}$$

Where, the subscripts i, j indicated the location of an asperity.

The equivalent radius of an asperity is the reciprocal of equivalent curvature and is shown as

$$r_{s,t} = \frac{2}{K} \tag{B.4}$$

Therefore, the mean asperity radius of the contact region is

$$r_s = \frac{1}{Q}\sum_{t=1}^{Q} r_{s,t} \tag{B.5}$$

Where, Q is the total number of asperities.

References

[1] Santus C, Beghini M, Bartilotta I, Facchini M. Surface and subsurface rolling contact fatigue characteristic depths and proposal of stress indexes. Int J Fatigue 2012. doi:10.1016/j.ijfatigue.2012.06.012.

[2] Wen S, Huang P. Principles of Tribology. 2011. doi:10.1002/9781118062913.

[3] Warhadpande A, Sadeghi F, Kotzalas MN, Doll G. Effects of plasticity on subsurface initiated spalling in rolling contact fatigue. Int J Fatigue 2012. doi:10.1016/j.ijfatigue.2011.08.012.

[4] Palmgren A, Lundberg G. Dynamic capacity of rolling bearings. J Appl Mech 1949.

[5] Ioannides E, Harris TA. A New Fatigue Life Model for Rolling Bearings. J Tribol 2009. doi:10.1115/1.3261081.

[6] Zaretsky E.Y. Fatigue criterion to system design, life, and reliability. J Propuls Power 1987. doi:10.2514/3.22955.

[7] Gupta PK, Oswald FB, Zaretsky E V. Comparison of Models for Ball Bearing Dynamic Capacity and Life. Tribol Trans 2015. doi:10.1080/10402004.2015.1038860.

[8] Gupta PK, Zaretsky E V. New Stress-Based Fatigue Life Models for Ball and Roller Bearings. Tribol Trans 2018. doi:10.1080/10402004.2017.1319524.

[9] Zhu D, Ren N, Wang QJ. Pitting Life Prediction Based on a 3D Line Contact Mixed EHL Analysis and Subsurface von Mises Stress Calculation. J Tribol 2009. doi:10.1115/1.3195040.

[10] Hamrock BJ, Dowson D. Isothermal Elastohydrodynamic Lubrication of Point Contacts: Part III—Fully Flooded Results. J Lubr Technol 1977. doi:10.1115/1.3453074.

[11] Liu Y, Wang QJ, Wang W, Hu Y, Zhu D. Effects of Differential Scheme and Mesh Density on EHL Film Thickness in Point Contacts. J Tribol 2006. doi:10.1115/1.2194916.

[12] Venner CH, Lubrecht AA. Multigrid techniques: A fast and efficient method for the numerical simulation of elastohydrodynamically lubricated point contact problems. Proc Inst Mech Eng Part J J Eng Tribol 2000. doi:10.1243/1350650001543007.

[13] Venner CH, ten Napel WE, Bosma R. Advanced Multilevel Solution of the EHL Line Contact Problem. J Tribol 1990. doi:10.1115/1.2920277.

[14] Patir N, Cheng HS. Application of Average Flow Model to Lubrication Between Rough Sliding Surfaces. J Lubr Technol 1977. doi:10.1115/1.3453329.

[15] Patir N, Cheng HS. An Average Flow Model for Determining Effects of Three-Dimensional Roughness on Partial Hydrodynamic Lubrication. J Lubr Technol 1978. doi:10.1115/1.3453103.

[16] Masjedi M, Khonsari MM. Film Thickness and Asperity Load Formulas for Line-Contact Elastohydrodynamic Lubrication With Provision for Surface Roughness. J Tribol 2012. doi:10.1115/1.4005514.

[17] Masjedi M, Khonsari MM. On the effect of surface roughness in point-contact EHL: Formulas for film thickness and asperity load. Tribol Int 2015. doi:10.1016/j.triboint.2014.09.010.

[18] Hu Y-Z, Zhu D. A Full Numerical Solution to the Mixed Lubrication in Point Contacts. J Tribol 2000. doi:10.1115/1.555322.

[19] Zhu D. Effect of surface roughness on mixed EHD lubrication characteristics. Tribol Trans 2003. doi:10.1080/10402000308982598.

[20] Zhu D, Hu YZ. A computer program package for the prediction of EHL and mixed lubrication characteristics, friction, subsurface stresses and flash temperatures based on measured 3-d surface roughness. Tribol Trans 2001. doi:10.1080/10402000108982471.

[21] Wang X, Liu Y, Zhu D. Numerical Solution of Mixed Thermal Elastohydrodynamic Lubrication in Point Contacts With Three-Dimensional Surface Roughness. J Tribol 2016. doi:10.1115/1.4032963.

[22] Pu W, Wang J, Zhu D. Progressive Mesh Densification Method for Numerical Solution of Mixed Elastohydrodynamic Lubrication. J Tribol 2015. doi:10.1115/1.4031495.

[23] He T, Zhu D, Wang J, Jane Wang Q. Experimental and Numerical Investigations of the Stribeck Curves for Lubricated Counterformal Contacts. J Tribol 2016. doi:10.1115/1.4034051.

[24] Zhang YZ, Kovalev A., Meng YG, Combined effect of boundary layer formation and surface smoothing on friction and wear rate of lubricated point contacts during normal running-in processes. Friction, 2018. Doi:10.1007/s40544-018-0228-4.

[25] Wang WZ, Wang H, Liu YC, Hu YZ, Zhu D. A comparative study of the methods for calculation of surface elastic deformation. Proc Inst Mech Eng Part J: J Eng Tribol 2003. doi:10.1243/13506500360603570.

[26] Hu YZ, Barber GC, Zhu D. Numerical analysis for the elastic contact of real rough surfaces. Tribol Trans 1999. doi:10.1080/10402009908982240.

[27] Bair S, Winer WO. A Rheological Model for Elastohydrodynamic Contacts Based on Primary Laboratory Data. J Lubr Technol 1979. doi:10.1115/1.3453342.

[28] Liu H, Liu H, Zhu C, He H, Wei P. Evaluation of Contact Fatigue Life of a Wind Turbine Gear Pair Considering Residual Stress. J Tribol 2018. doi:10.1115/1.4039164.

[29] Wang Z, Jin X, Zhou Q, Ai X, Keer LM, Wang Q. An Efficient Numerical Method With a Parallel Computational Strategy for Solving Arbitrarily Shaped Inclusions in Elastoplastic Contact Problems. J Tribol 2013. doi:10.1115/1.4023948.

[30] Liu S, Wang Q, Liu G. A versatile method of discrete convolution and FFT (DC-FFT) for contact analyses. Wear 2000. doi:10.1016/S0043-1648(00)00427-0.

[31] Yan X, Zhang Y, Xie G, Qin F, Zhang X. Effects of spinning on the mixed thermal elastohydrodynamic lubrication and fatigue life in point contacts. Proc Inst Mech Eng Part J J Eng Tribol 2019. doi:10.1177/1350650119847404.

[32] Wang ZJ, Wang WZ, Wang H, Hu YZ. Stress analysis on layered materials in point Elastohydrodynamic-Lubricated contacts. Tribol Lett 2009. doi:10.1007/s11249-009-9452-4.

[33] Sayles RS, Thomas TR. Measurements of the Statistical Microgeometry of Engineering Surfaces. J Lubr Technol 1979. doi:10.1115/1.3453384.

[34] Liu S, Wang Q. Studying Contact Stress Fields Caused by Surface Tractions With a Discrete Convolution and Fast Fourier Transform Algorithm. J Tribol 2002. doi:10.1115/1.1401017.